Pharm Res (2014) 31:1059–1070
DOI 10.1007/s11095-013-1227-9

RESEARCH PAPER

A Novel Three-Dimensional Large-Pore Mesoporous Carbon Matrix as a Potential Nanovehicle for the Fast Release of the Poorly Water-soluble Drug, Celecoxib

Yanzhuo Zhang • Hong Wang • Chuanjun Li • Baoxiang Sun • Yu Wang • Siling Wang • Cunqiang Gao

Received: 24 July 2013 / Accepted: 3 October 2013 / Published online: 28 November 2013

ABSTRACT

Purpose A novel mesocellular carbon foam (MSU-FC) with a large pore size and a three-dimensional porous structure for the oral delivery of poorly water-soluble drugs was prepared. The goal of this study was to improve *in vitro* dissolution and *in vivo* absorption of celecoxib (CEB), a model drug, by means of novel carbon-based nanoparticles prepared from the MSU-FC matrix.

Methods The MSU-FC matrix was synthesized by an inverse replica templating method using mesocellular silica template. A solvent immersion/evaporation method was used to load the drug molecules. The drug-loaded nanoparticles were characterized for morphology, surface area, particle size, mesoporous structure, crystallinity, solubility and dissolution. The effect of MSU-FC on cell viability was measured using the MTT conversion assay. Furthermore, the oral bioavailability of CEB-loaded MSU-FC in fasted rats was compared with that of the marketed product.

Results Our results demonstrate that CEB incorporation into the prepared MSU-FC resulted in an approximately 9-fold increase in aqueous solubility in comparison with crystalline CEB. MSU-FC produced accelerated immediate release of CEB in comparison with crystalline CEB (pure CEB powder or marketed formulation) and the drug-loaded conventional mesoporous carbon particles. The relative bioavailability of CEB for CEB-loaded MSU-FC was 172%. In addition, MSU-FC nanoparticles exhibited very low toxicity.

Conclusions The MSU-FC nanomatrix has been shown to be a promising drug delivery vehicle for improving the dissolution and biopharmaceutical characteristics of poorly water-soluble drugs.

KEY WORDS carbon matrix · crystallinity · cytotoxicity · dissolution · drug absorption

Y. Zhang (✉) • Y. Wang
Department of Pharmaceutics, Xuzhou Medical College, P.O. Box 62, No. 209, Tongshan Road
Xuzhou 221004, China
e-mail: yanzhuozhang@126.com

H. Wang • S. Wang
Department of Pharmaceutics, School of Pharmacy
Shenyang Pharmaceutical University, No. 103, Wenhua Road
Shenyang 110016, China

C. Li • B. Sun • C. Gao
Jiangsu Hengrui Medicine Co. Ltd., No. 11
Changjiang Road, Lianyungang 222047, China

INTRODUCTION

The application of combinatorial chemistry and high-throughput screening has led to the discovery of numerous new chemical entities (NCE) as potential therapeutic agents. However, problems of poor solubility in the gastrointestinal (GI) fluid, insufficient dissolution in the GI tract and poor oral bioavailability are often causes that result in the rejection of potentially valuable drug candidates as pharmaceutical products (1,2). At present it is estimated that as much as 70% of NCE are poorly soluble in aqueous media and many even in organic media, and as much as 40% of commercial immediate-release oral formulations are considered practically insoluble in water (3). Without a sufficiently high level of active pharmaceutical ingredient (API) in the GI fluid, the API may not be effectively transported *via* the epithelia present along the GI tract, resulting in low systemic absorption (4). Hence, one of the major challenges of the pharmaceutical industry is to develop strategies to improve the aqueous solubility and dissolution rate of poorly water-soluble drugs. This is particularly pertinent to drug candidates within class II of the Biopharmaceutics Classification System (poorly water-soluble but highly permeable), where dissolution velocity is the rate-limiting step for absorption (5,6). As a result, much research has been conducted into methods of improving the solubility and dissolution rate to increase the oral bioavailability of poorly water-soluble drugs (7,8).

Over recent decades, nano-strategies have been employed to improve the delivery efficiency of poorly water-soluble

drugs (9,10), such as drug nanocystals (11), nanosuspension (12), nanoemulsions (13), solid lipid nanoparticles (14) and polymeric nanoparticles (15). These formulation approaches have been proven to play a vital role in the whole process of drug development and have provided opportunities for revitalizing marketed products with suboptimal delivery. The use of mesoporous matrices to form stable nanometer-sized drug-loaded particles is a relatively newer formulation strategy (16,17). Mesoporous nanomatrices offer several advantages for drug delivery over polymeric nanoparticles, including unique ordered porosity at the nanoscale, tunable morphology and pore size, a large surface area to highly disperse the drug molecules, a high drug loading capacity, and good thermal stability (18–20). During the past few years, the application of mesoporous silica materials as prospective vehicles for oral drug delivery has been widely studied to improve the dissolution properties of poorly water-soluble drugs (21–23). The ability of mesoporous materials to enhance the solubility and dissolution rate of the incorporated drug is due to their small nanopores (usually 2–50 nm in diameter), which can change the crystalline drug to an amorphous state and reduce the particle size of the drug to the low nanometer range (21,24). Carbon-based mesoporous matrices, synthesized by an inverse replica templating method using inorganic templates, are nanostructured materials that have a larger pore volume (25), greater adsorption capacity (26) and a higher surface area compared with other mesoporous materials and, so, they should provide a higher drug loading capacity (27). All of these properties demonstrate the potential and advantages of using mesoporous carbon matrices in drug delivery systems. However, there are still few reports about the enhancement of the dissolution of poorly aqueous-soluble drugs using synthetic mesoporous carbon materials (28,29).

Regarding the application of mesoporous carbon matrices, several properties of the materials affect the loading degree and release rate of the incorporated drug, such as the surface area, pore size, pore volume, pore geometry, particle morphology and primary particle size (30–32). Although conventional mesoporous carbon matrices have very large surface areas and large pore volumes, and have been proved to efficiently incorporate drugs with a small molecular weight, they are not suitable for fast release of the incorporated drug in the nanopore channels (28,33,34). This is mainly due to their small mesopore size (below 5 nm), which limits the rapid and easy diffusion of the drug molecules into the dissolution medium. Notably, MSU-FC with a large pore size (above 20 nm) and three-dimensional porous structure is thought to have advantages over other carbon matrices having two-dimensional arrays of small pores (25,26,35,36), mainly because it facilitates the transport of drugs from the inner pores to the outer dissolution medium, thus leading to faster drug release. To the best of our knowledge, this three-dimensional large-pore mesoporous carbon matrix has not been reported yet as a potential vehicle for the oral delivery of poorly water-soluble drugs.

In this paper, we describe the successful synthesis of a three-dimensional large-pore MSU-FC nanomatrix as an oral drug carrier and loaded a model drug into its pore channels. CEB (Fig. 1), a selective cyclo-oxygenase-2 enzyme inhibitor, is widely used for the treatment of osteoarthritis, rheumatoid arthritis and acute pain. CEB is weakly acidic with a p*K*a of 11.1. It is classified in the BCS system as a class II drug with low aqueous solubility (about 5 μg/ml) and high permeability (37). It has been reported that the oral bioavailability of the conventional CEB capsule ranges from 22 to 40% in dogs and the extent of drug absorption is limited by the dissolution rate (38). CEB was used as a model drug in the present study due to its low aqueous solubility and poor oral bioavailability. The aim of the present study was to improve *in vitro* dissolution and *in vivo* absorption of CEB by means of novel carbon-based nanoparticles prepared using the three-dimensional large-pore MSU-FC nanomatrix. The physicochemical properties of the drug-loaded nanoparticles were systematically studied using nitrogen adsorption, scanning electron microscopy (SEM), transmission electron microscopy (TEM), differential scanning calorimetry (DSC), powder X-ray diffraction (PXRD), high performance liquid chromatography (HPLC) and solubility measurements. Furthermore, the *in vitro* drug dissolution and *in vivo* drug absorption were confirmed and the possible mechanism of enhancement of the dissolution and oral bioavailability was investigated.

MATERIALS AND METHODS

Materials

Furfuryl alcohol, aluminium chloride and sodium lauryl sulfate (SLS) were obtained from Nanjing Reagent Co., Ltd. (Nanjing,

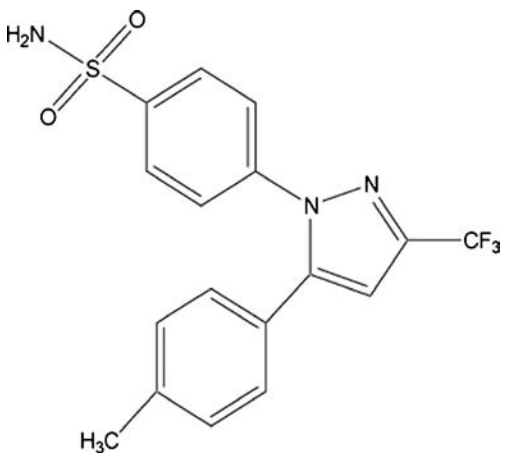

Fig. 1 Chemical structure of CEB.

China). Pharmaceutical-grade CEB (purity ≥98%) and triamcinolone acetonide (purity ≥98%) were kindly donated from Hengrui Pharmaceutical Co., Ltd. (Jiangsu, China). Poloxamer 188 was purchased from BASF (Ludwigshafen, Germany). 3-(4,5-Dimethylthiazol-2-yl)-2,5-diphenyltetrazolium bromide (MTT) and Dulbecco's modified Eagle's medium (DMEM) were purchased from Sigma-Aldrich (St. Louis, MO, USA). Sodium carboxymethyl cellulose was purchased from FMC BioPolymer (Philadelphia, PA, USA). Commercial Celebrex® capsules (Pfizer) containing 50 mg of active drug were purchased from a local pharmacy. Water was obtained from a Millipore Milli-Q filtration/purification system (Billerica, MA, USA) and all other reagents were of analytical or chromatographic grade.

Preparation of MSU-FC and CMK-3 (Carbon Molecular Sieve-3) Mesoporous Matrices

The ordered mesoporous carbon matrix was prepared using furfuryl alcohol as a carbon source and mesoporous silica as a hard template, as reported by An and co-workers (35) with some modifications. Mesostructured cellular foam silica (MCF) and Santa Barbara amorphous-15 silica (SBA-15) were synthesized as described in the literature (39). To prepare MCF matrix, 3.6 g Pluronic 123 was dissolved in 135 ml 1.6 M hydrochloric acid solution. Then, 0.6 g cetyltrimethyl ammonium bromide, 2.4 ml 1,3,5-trimethylbenzene and 0.038 g ammonia tetrafluoride were added to the Pluronic 123 solution, the mixture was stirred for 120 min, and 7.5 g tetraethyl orthosilicate was added to this solution. After 5 min stirring, the reaction mixture was kept under static conditions at 38°C for 20 h. The resulting colloidal mixture was crystallized at 120°C for over a day. The resulting white precipitate was filtered, washed, and calcined at 600°C for 5 h. To prepare SBA-15 matrix, 4.0 g Pluronic 123 was dissolved in 150 ml 1.6 M hydrochloric acid solution. Subsequently, 8.6 g tetraethyl orthosilicate was added to this solution with stirring at 40°C. After 24 h stirring, the obtained white precipitate was filtered, washed, and calcined at 600°C for 5 h.

For the synthesis of the MSU-FC matrix, 2.0 g MCF was suspended in 16 ml of a 0.1 M ethanolic solution of aluminium chloride, and ultrasonicated for 30 min. After the solvent was completely evaporated in a N1000 rotary evaporator (Eyela, Japan) at 60°C, the resulting powder was calcined at 600°C in air for 4 h to obtain the aluminated MCF template. Then, 500 mg of the aluminated MCF was infiltrated with 0.6 ml furfuryl alcohol by the incipient wetness technique at room temperature. The reaction mixture was then heated to 90°C in a DGT-10 drying oven (Haier, China) for 24 h to allow the aluminium-catalyzed polymerization of furfuryl alcohol. The obtained composite was filtered, rinsed thoroughly with ethanol, and heated at 900°C for 5 h to carbonize the polymer in an argon atmosphere. The carbonized sample was stirred in a 5% hydrofluoric acid solution at room temperature for 4 h to completely remove the aluminated MCF template. Finally, the resulting product was impregnated with a mixture of concentrated sulfuric and nitric acids for 12 h, filtered with a 0.45 μm Millipore filter membrane (Billerica, MA, USA), washed with ethanol, and dried under vacuum. CMK-3 was synthesized in the same way as MSU-FC, except for the use of 500 mg SBA-15 as a hard template and 0.45 ml furfuryl alcohol.

Loading CEB into the MSU-FC and CMK-3 Matrices

A solvent immersion/evaporation method was used to load the drug molecules into the pores of the MSU-FC and CMK-3 matrices. Typically, 600 mg MSU-FC was immersed in 40 ml 0.27 M CEB solution in ethanol (containing 0.3% poloxamer 188) in a stoppered flat-bottom flask. Then, the particle suspensions were ultrasonicated for a few minutes and stirred for 24 h using a HJ-A6 magnetic stirring plate (Runhua, China) to achieve maximum loading of MSU-FC in the pore channels. Subsequently, the obtained CEB-impregnated MSU-FC particles were vacuum filtered from the solution using a 0.45 μm syringe-driven filter unit (Sartorius, AG, Germany). The moist powder was then dried at 50°C under reduced pressure (10^{-3} bar) for over a day in order to remove the solvent completely. The dried composite samples were referred to as CEB-MSU-FC. The procedure for CEB loading into CMK-3 was similar to that used for loading MSU-FC. The CEB-loaded samples were referred to as CEB-CMK-3.

Measurement of Size and Morphology

Representative TEM images of the particles were recorded on a JEM-100CX II microscope (JEOL, Japan) operated at a voltage of 200 kV. Prior to imaging, each sample was dispersed in water by sonication and then deposited on a carbon-coated copper grid. SEM images of the unloaded and CEB-loaded particles were acquired with a SUPRA 35 microscope (Carl Zeiss, Germany). Prior to imaging, the samples were deposited on a sample holder using an adhesive carbon tape and then sputter-coated with a thin layer (~ 10 nm thick) of platinum. The particle size of the prepared MSU-FC particles was determined using a Nicomp 380 dynamic light scattering (DLS) instrument (PSS, USA). The samples were dispersed in water and measured at scattering angle of 90° at 25°C.

Measurement of Specific Surface Area and Pore Volume

Nitrogen adsorption–desorption isotherms and pore characterizations of the prepared samples were recorded at −196°C over a wide relative pressure range from 0.01 to 0.995 atm using an ASAP 2020 gas adsorption analyzer (Micromeritics,

USA). Before measurement, the CEB-loaded particles and the pure CEB powder were degassed at 50°C overnight under high vacuum. The total surface area was calculated using the Brunauer–Emmett–Teller equation from nitrogen adsorption data over the relative pressure range between 0.05 and 0.2. The average pore diameter was obtained from the adsorption branch of the isotherm using the Barrett–Joyner–Halenda (BJH) method. The total pore volume was determined from the volume adsorbed at a relative pressure of 0.98.

Solid-State Characterization by PXRD and DSC

The crystallinity of the CEB-loaded samples and also the pure CEB was assessed by PXRD. PXRD profiles of the prepared samples were recorded on an AXS D8 Advance diffractometer (Bruker AXS GmbH, Germany), equipped with a Cu-Ka radiation point source ($\lambda = 1.7902$ Å). The equipment was operated at a voltage of 40 kV and a current of 30 mA. The powder samples were gently consolidated in an aluminium holder and measured over a 2θ angle range from 5 to 40°. The scanning rate was 4°/min using a sampling step of 0.02°. Each formulation was analyzed in duplicate.

In addition to PXRD measurements, DSC was performed to characterize the physical state of the pure CEB and CEB-loaded samples. Measurements were performed on a modulated temperature DSC 1 Stare apparatus equipped with a refrigerated cooling system (Mettler Toledo, Switzerland). The temperature scale and heat flow were calibrated with indium. A sample of approximately 5 mg was accurately weighed, placed in an aluminum pan, and crimped with an aluminum lid. Testing was performed at temperatures increasing from 50 to 200°C at a rate of 10°C/min. Dry nitrogen at a flow rate of 50 ml/min was used as the purge gas.

In Vitro Quantification of CEB

All samples from the *in vitro* experiments (drug loading capacity, solubility measurements and *in vitro* dissolution study) were assayed using an Agilent 1100 Series instrument (Agilent Technologies, USA). The chromatographic system consisted of a binary pump (G1312A), a temperature-controlled column compartment (G1316A), an autosampler (G1313A), and a variable spectrophotometric detector (G1314B). The analysis of CEB was performed on a 200×4.6 mm Zorbax C_{18} analytical column (Agilent Technologies, USA) at 40°C, eluting with acetonitrile and 10 mM phosphate buffer solution (55/45%, v/v) at a flow rate of 1.0 ml/min. The variable spectrophotometric detector was set at a wavelength of 252 nm. The data were collected and processed using HPLC 1100 ChemStation software. The calibration curve of CEB was linear ($r^2 = 0.99$) over the concentration range 0.5–40 μg/ml. Parameters validated included precision (intra-day and inter-day) and accuracy. Both the intra- and inter-day relative standard deviations (RSD) of the quality control (QC) standards were less than 4% over the selected range. The high accuracy of the method was confirmed with recovery values of 98–102%.

Drug Loading Capacity Study

The CEB content of the carbon-based formulation was determined by dissolving an accurately weighed amount of CEB-loaded composites (about 10 mg) in 200 ml methanol. These suspensions were ultrasonicated for 30 min and subsequently put in a rotary mixer for 24 h. Afterwards, the carbon matrix was separated from the CEB solution by centrifugation (5,600×g, 10 min). The supernatant layer was taken, suitably diluted with mobile phase and then the drug concentration was determined by HPLC. All measurements were performed in triplicate. The drug loading was calculated using the following Eq. (1):

$$\text{Drug loading (\%)} = (\text{weight of drug incomposites}/\text{weight ofcomposites}) \times 100 \quad (1)$$

Aqueous Solubility Study

The saturation solubility of CEB in deionized water and phosphate buffer solution (PBS, pH 6.8) was determined using the shake-flask method. Briefly, excess amount of CEB was added to 40 ml capped vials containing 20 ml deionized water and PBS. The capped vials were vortexed and then placed in an NRV-200 shaker incubator (Nanrong Lab-Line Instrument, China) at 37±0.5°C, 100 rpm for 72 h. After equilibrium was reached, 5 ml suspension was passed through a 0.45 μm syringe driven filter unit. The concentration of CEB in the filtrate was determined by HPLC as described above.

In Vitro Dissolution Study

The dissolution test under sink conditions was performed using a USP II paddle method with an AT7 Smart offline dissolution tester (Sotax, Switzerland). The rotational speed for the paddles was set at 50 rpm, 900 ml PBS (pH 6.8, containing 1.0% SLS) or hydrochloric acid solution (pH 1.2, containing 1.0% SLS) was used as the dissolution medium in each of the vessels and the temperature was kept constant at 37°C. The CEB-loaded samples (equivalent to 50 mg CEB) and 50 mg pure CEB powder were exposed to the dissolution medium. Then, 4 ml samples were taken and immediately replaced with fresh dissolution medium after 5, 10, 15, 20, 30, 45, 60 and 120 min. The withdrawn samples were passed through a 0.45 μm syringe driven filter unit discarding the first 1–2 ml of filtrate. The rest of the filtrate was diluted with mobile phase and subsequently analyzed using a reversed phase HPLC system with UV detection.

In Vitro Cytotoxicity Assay

The effect of MSU-FC (or CMK-3) on cell viability was measured at selected concentrations using the MTT conversion assay. Caco-2 cells (American Type Culture Collection, Manassas, VA, USA) were seeded into 96-well plates at a density of 1×10^4 cells per well and incubated for about 72 h to reach confluence. The culture was maintained at 37°C in a 5% CO_2 atmosphere and 95% relative humidity (BBD 6220 CO_2 Incubator, Thermo Scientific, Germany). Then, the culture medium (DMEM) was removed from the wells and replaced with 100 μl fresh DMEM containing different concentrations of MSU-FC (or CMK-3) matrix (10, 20, 50, 75, 100 and 150 μg/ml). Caco-2 cells cultured in the absence of carbon matrix acted as controls. After incubation for 24 h, the wells were washed three times with PBS (pH 7.4) to remove particle suspensions (for test cells) or blank culture medium (for control cells), and the plates were equilibrated at room temperature for about 30 min. Then, 10 μl MTT solution (5 mg/ml) was added to each well and the cells were further incubated for 6 h. Subsequently, the MTT medium was removed and 100 μl DMSO was added to each well to dissolve the formazan crystals. Finally, the absorbance of the resulting formazan solution was measured at 570 nm using a Synergy™ HT microplate reader (BioTek Instruments Inc, USA), and the cell survival (%) was calculated as follows:

$$\text{Cell survival (\%)} = (\text{Absorbance oftest}/\text{Absorbance of control}) \times 100 \quad (2)$$

Solid-State Stability Study

To assess the solid-state stability of drug-loaded MSU-FC, the accelerated stability test was performed at 40°C and 75% relative humidity. Each sample was put into a glass vial and sealed, which was then placed in a LHH-SGG constant temperature and humidity chamber (Guangjun, China). The samples were obtained at designated time points (1, 2, 3 and 6 months), and the crystallinity of drug-loaded MSU-FC was monitored by PXRD.

Oral Bioavailability Studies

Animal Procedures and Sample Collection

The *in vivo* experiment was performed using male Sprague–Dawley rats (body weight about 300–350 g, the Experimental Animal Center of Nanjing University, Nanjing, China). The rats were kept in ventilated cages and maintained on a standard diet with free access to water. All animal experiments were performed according to the institutional animal protocol guidelines approved by Nanjing University. The animals were divided randomly into 3 groups of 6 animals each. Prior to the experiment, the rats were deprived of food but provided with free access to water for 12 h. The powder from commercial CEB capsules, pure CEB powder and CEB-loaded samples were suspended in 2 ml 0.3% sodium carboxymethyl cellulose solution and given intragastrically at a dose of 10 mg/kg. Blood samples (approximately 0.2 ml) were collected from the orbital sinus into tubes containing potassium EDTA anticoagulant pre-dosing and 0.5, 1, 1.5, 2, 2.5, 3, 4, 6, 8, 12, 24 and 48 h post-dosing. Plasma was separated by centrifugation at 3,000×g for 10 min and stored at approximately −70°C until required for further analysis. Triamcinolone acetonide was used as an internal standard during the sample preparation. Then, 100 μl plasma samples were pipetted into 7 ml centrifuge tubes and spiked with 10 μl internal standard (20 μg/ml triamcinolone acetonide in methanol). Subsequently, each sample was extracted with 5 ml ethyl acetate by vortex mixing for 4 min. After centrifugation at 6,000×g for 10 min, the upper organic layer was transferred to a clean centrifuge tube and dried under nitrogen at 40°C in a water bath. The residue was reconstituted in 200 μl mobile phase and then centrifuged at 6,000×g for 5 min. The supernatant of each sample was transferred to an autosampler vial and a 20 μl aliquot was injected into the HPLC system for CEB quantification.

HPLC Plasma Assay for CEB

All samples from the *in vivo* experiment were assayed using a Shimadzu LC-10AT Series instrument (Shimadzu Scientific Instruments, Japan). The HPLC system consisted of a LC-10ATvp binary pump, a SCL-10Avp system controller, a CO-IV column oven and a SPD-10Avp UV/VIS detector. The HPLC separation was performed using a 200×4.6 mm reversed-phase Shim-pack VP-ODS C_{18} column (Shimadzu, Japan) with a 4×3.0 mm security guard C_{18} column (WondaGuard, Shimadzu, Japan) at 40°C, eluting with methanol and 10 mM potassium dihydrogen phosphate solution (adjusted to pH 3.0 with phosphoric acid) in a volume ratio of 70/30 (v/v) at a flow rate of 1.0 ml/min. The UV/VIS detector was set at a wavelength of 252 nm. The data were collected and processed using Shimadzu CLASS-VP software. The internal standard triamcinolone acetonide and CEB had retention times of 6.2 and 11.7 min, respectively. The limit of detection (LOD) and the limit of quantification (LOQ) of this analytical method was 10 ng/ml and 20 ng/ml, respectively. A linear calibration curve over the concentration range 0.04–5 μg/ml was constructed with recovery of the standard within an acceptable range of 90.0–110.0%.

Pharmacokinetic Analysis

The area under the plasma concentration *versus* time curve from time zero to time t h (AUC_{0-t}) was calculated using

noncompartmental analysis (DAS 2.1.1; Mathematical Pharmacology Professional Committee of China). The maximum plasma concentration of the drug (C_{max}) and the time taken to reach the maximum plasma concentration (T_{max}) were directly obtained from the plasma data. The relative bioavailability (*Fr*) was estimated by dividing the AUC_{0-t} of the test formulation by that of the commercial formulation.

Statistical Analysis

Statistical analysis was performed using the statistical package for social sciences (SPSS version 17.0). All values were expressed as the means ± SD. The statistical differences between two groups were evaluated by Student's independent sample *t*-test and expressed as a one-way *p* value. Statistical probability (*p*) values less than 0.05 were considered significantly different.

RESULTS AND DISCUSSION

Morphology and Porous Structure of the Prepared Samples

The morphology, particle size and mesoporous structure of the prepared MSU-FC matrix were investigated by TEM. The MSU-FC nanoparticles were spherical in shape with an average particle size of about 800–900 nm (Fig. 2a). The average particle size was also determined by DLS (830 ± 116 nm) and was in reasonable agreement with the values determined by TEM. Figure 2b shows the details of the organization of the porous system. The MSU-FC matrix had a three-dimensional, interconnected pore structure and consisted of randomly oriented spherical cells, similar to that of the mesoporous silica MCF template. Significantly, the TEM images also showed that the pore diameter (approximately 25 nm) of MSU-FC was much larger than that of conventional mesoporous carbon materials (with an average nanopore diameter of 2–6 nm), which is consistent with the average pore diameters obtained from the nitrogen adsorption measurements (Table I). The larger pore diameter of MSU-FC could be attributed to MCF was used as the template. A similar three-dimensional continuous mesopore structure in Fig. 2c, demonstrates that the mesoporous structure of MSU-FC was substantially maintained after drug loading. As shown by the SEM analyses, the morphology of the drug-loaded MSU-FC was the same as the MSU-FC matrix, and no separated particles of drug were observed (Fig. 2d). The SEM and TEM images of drug-loaded MSU-FC indicate that the drug was largely amorphous and molecularly dispersed into the MSU-FC matrix, as confirmed by the PXRD, DSC and nitrogen adsorption studies. As seen in Fig. 3a, CMK-3 was aggregated with a wheat-like macrostructure consisting of many tube-like structures with a length of 1–2 μm and a diameter of about 0.4 μm. The representative TEM micrograph shown in Fig. 3b shows that CMK-3 had a highly ordered mesoporous structure with rodlike walls; in particular, highly two-dimensional ordered pore channels were arrayed along the walls, which is the reverse hexagonal structure of SBA-15. The average pore diameter of CMK-3 was approximately 5 nm. The SEM micrograph (Fig. 3c) shows that pure CEB consisted of predominantly needle-shaped crystals between 2 and 50 μm in size. It can be seen that the drug-loaded CMK-3 also had the tube-type morphology of the CMK-3 matrix, and no crude drug crystals were present (Fig. 3d).

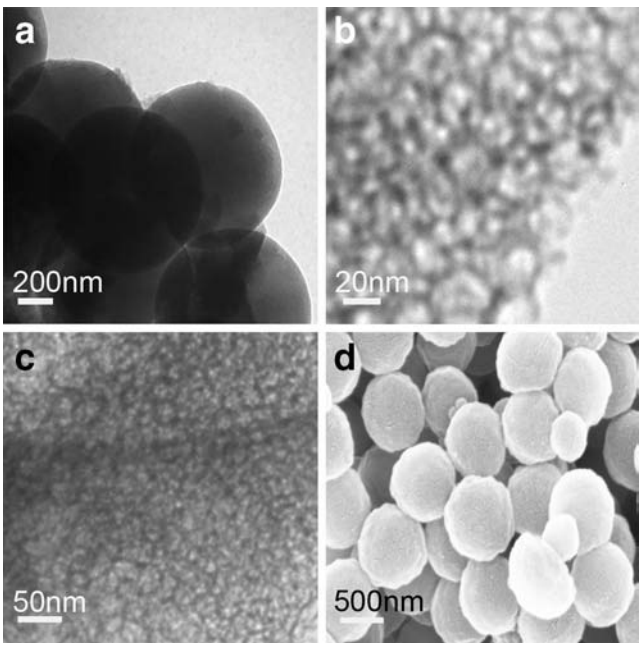

Fig. 2 TEM micrographs of (**a**) MSU-FC, (**b**) MSU-FC (enlarged) and (**c**) CEB-MSU-FC; SEM micrograph of (**d**) CEB-MSU-FC.

Specific Surface Area and Pore Size Distribution of the Prepared Samples

The nitrogen adsorption-desorption isotherms of the prepared CMK-3 and MSU-FC materials are presented in Fig. 4, along with their corresponding pore size distributions calculated using the BJH method. The measured isotherms for both samples are Type IV isotherms according to the IUPAC classification, with H1 hysteresis loops, characteristic of mesoporous materials. As seen in Fig. 4d, only one peak appeared in the range 4–6 nm of the pore size distribution curve of CMK-3, and no large mesopores were present, suggesting that small mesopores must be predominant in this porous system. For the MSU-FC samples, the cellular pore sizes were determined from the adsorption branches of the isotherms and window sizes were determined from the desorption branches (35,40). As shown in the pore size distribution

Table I Pore Properties and Drug Loading of the Samples ($n = 3$)

Sample	SBET (m^2/g)	Vt (cm^3/g)	wBJH (nm)	Wall thickness (nm)	Drug loading (%)
MSU-FC	1257.1 ± 10.6	1.94 ± 0.12	26.8 ± 3.1	3.6 ± 1.2	–
CMK-3	1623.5 ± 15.7	1.53 ± 0.07	4.9 ± 1.5	2.4 ± 0.7	–
CEB-MSU-FC	271.8 ± 9.5	0.38 ± 0.04	20.4 ± 2.8	4.9 ± 1.8	42.9 ± 1.1
CEB-CMK-3	161.0 ± 23.7	0.29 ± 0.11	1.6 ± 0.3	3.9 ± 1.6	36.5 ± 0.4

SBET BET specific surface area; Vt total pore volume; wBJH BJH pore diameter

curves of MSU-FC in Fig. 4e and f, the peaks at 26.8 and 17.4 nm could be ascribed to the cellular pore diameter and the window size of the MSU-FC matrix, respectively. The textural properties of CMK-3 and MSU-FC are listed in Table I. The larger pore volume and surface area (compared with those of other mesoporous materials, such as aluminum oxide, silica) indicated that the obtained MSU-FC matrix would be excellent if used as a host for storing more drug molecules in the drug delivery system (33,35). In addition, the successful incorporation of CEB into the pores of the carrier was also confirmed by nitrogen adsorption measurements. After drug loading, the pore diameter decreased to 20.4 nm and 1.6 nm for MSU-FC and CMK-3, respectively. The incorporation of CEB also decreased the BET specific surface area and total pore volume, which indicated that CEB was successfully incorporated into the pore channels of CMK-3 and MSU-FC. The drug loading capacity of MSU-FC was significantly higher than that of CMK-3 due to its relatively larger pore volume (the pore volume of MSU-FC was almost 1.3-fold greater than that of CMK-3). It is well known that the relatively high pore volume of mesoporous material enables it to achieve a high drug loading efficiency (16,33).

Solid-State Characterization

Solid state characterization with PXRD is a valuable analytical tool for understanding the amorphous and microcrystalline nature of complex structures. Figure 5 shows comparative diffractograms for pure CEB, the physical mixture (the mass ratio of CEB: MSU-FC was 1:1) and CEB-loaded samples. In the diffractogram of pure CEB, sharp peaks at a different 2θ angle of 14.6, 16.1, 19.5, 21.3 and 22.3° revealed the crystalline nature of CEB (Fig. 5a). For the physical mixture, diffraction peaks of CEB were also clearly visible which shows that there was no crystal change in CEB (Fig. 5d). However, no crystalline CEB was detected in both CEB-loaded samples (Fig. 5e and f). The absence of diffraction peaks owing to CEB in the PXRD analysis is evidence that the encapsulated drug CEB was molecularly well dispersed in both carbon matrices,

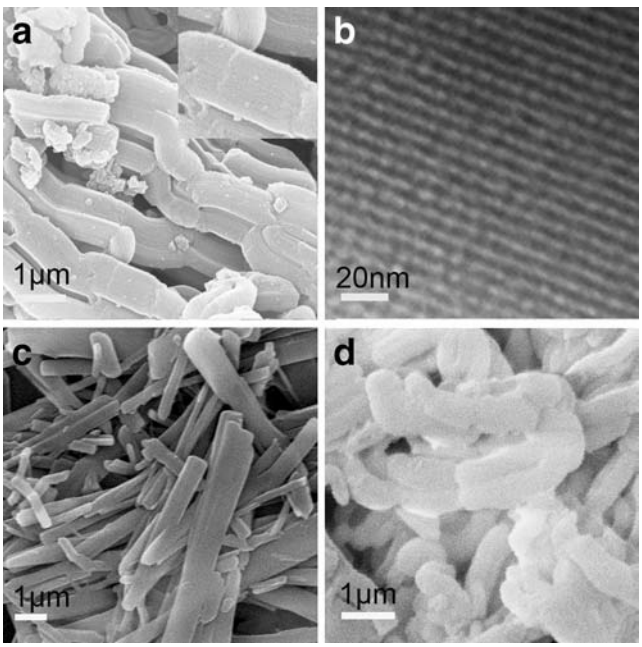

Fig. 3 SEM micrographs (**a**) CMK-3, (**c**) pure CEB and (**d**) CEB-CMK-3; TEM micrograph of (**b**) CMK-3.

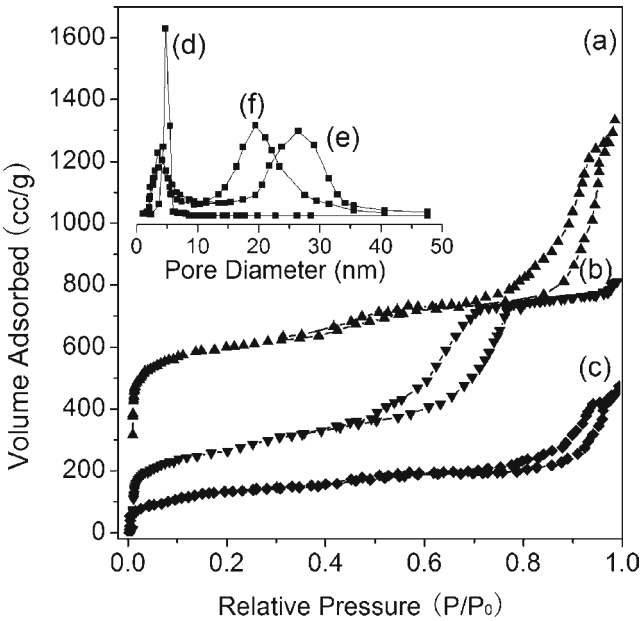

Fig. 4 Nitrogen adsorption/desorption isotherms of (*a*) MSU-FC, (*b*) CMK-3 and (*c*) CEB-MSU-FC. (*a*) was offset vertically by 500 (cm^3/g STP). Pore size distributions of (*d*) CMK-3, (e) MSU-FC (determined from the adsorption branch of the isotherm) and (*f*) MSU-FC (determined from the desorption branch of the isotherm).

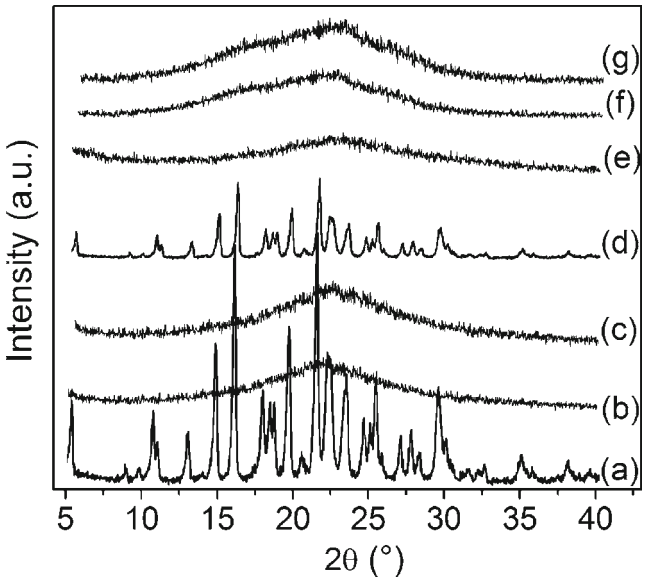

Fig. 5 PXRD patterns of (*a*) pure CEB, (*b*) MSU-FC, (*c*) CMK-3, (*d*) physical mixture, (*e*) CEB-CMK-3, (*f*) CEB-MSU-FC and (*g*) CEB-MSU-FC after 6 months of storage.

and complete drug amorphization was attained. It should be noted that CEB-loaded MSU-FC showed no sign of recrystallization during the storage time of 6 months (Fig. 5g). This can be largely attributed to the nanoscale pore channels of carbon matrix may effectively restrict drug recrystallization.

The presence or absence of crystalline drug was also confirmed by DSC analysis using the drug melting peak in the thermograms as an indication that CEB in crystalline form was present in the sample. The DSC thermograms of CEB, the physical mixture and CEB-loaded MSU-FC are shown in Fig. 6. Pure CEB showed a single sharp endothermic peak at

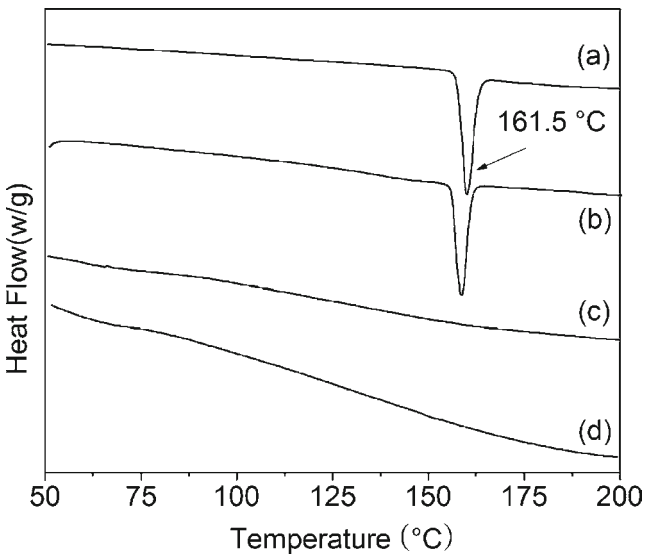

Fig. 6 DSC thermograms of (*a*) pure CEB, (*b*) physical mixture, (*c*) CEB-CMK-3 and (*d*) CEB-MSU-FC.

161.5°C (Fig. 6a, the enthalpy of fusion was 89.53 ± 1.40 J/g, $n = 3$), corresponding to its melting point and indicating its crystalline nature. A similar endothermic peak at 159°C (the enthalpy of fusion was 86.27 ± 2.11 J/g, $n = 3$) was also detected on the DSC curve of the physical mixture (Fig. 6b), suggesting that the drug was present in an unchanged crystalline state in the physical mixture. In contrast, the no endothermic peak of crystalline CEB was present in the DSC thermograms of both CEB-loaded samples (Fig. 6c and d), which indicated that the CEB entrapped in both carbon matrices was in an amorphous state. These results are in agreement with the PXRD results.

Solubility Study

Table II shows the saturation solubility measured for the pure CEB and CEB-loaded samples. The saturation solubility of pure CEB was about 4.2 ± 0.2 μg/ml in deionized water and 6.0 ± 0.2 μg/ml in PBS (pH 6.8), indicating that this drug is naturally poorly water-soluble. In contrast, both CEB-loaded samples significantly increased the CEB aqueous solubility compared with pure CEB. CEB-loaded MSU-FC demonstrated a saturation solubility of 36.5 ± 1.2 μg/ml in deionized water, about nine times higher than that of pure CEB. The differences in saturation solubility were mainly due to the differences in the solid state and particle size of CEB. On one hand, after CEB nanosizing by the pore channels of the two carriers, the state of the drug changed from a crystalline form to an amorphous form. It is well known that the amorphous state is the highest energy form of a solid material with no long-range molecular order (8,41). As a result of their high internal energy, amorphous materials generally have greater molecular motion and enhanced thermodynamic properties compared with the crystalline state (leading to a higher apparent solubility and dissolution rate). On the other hand, the particle size of the amorphous drug incorporated in the pore channels (nano-scale) was significantly reduced compared with that of pure CEB (micro-scale, as confirmed by SEM). A significantly reduced drug particle size increases the surface area and then the solubility according to the Ostwald–Freundlich and the Kelvin equations (10,11,42).

Table II Saturation Solubilities of Different CEB Formulations in Aqueous Media ($n = 3$)

Sample	Deionized water (μg/ml)	pH 6.8 PBS (μg/ml)
Pure CEB	4.2 ± 0.2	6.0 ± 0.2
Physical mixture	4.0 ± 0.1	5.7 ± 0.4
CEB-MSU-FC	36.5 ± 1.2*	52.5 ± 3.1*
CEB-CMK-3	33.7 ± 2.9*	54.0 ± 2.6*

* $P < 0.05$ compared with the pure CEB. There was no significant difference in saturation solubility between CEB-MSU-FC and CEB-CMK-3

In Vitro Drug Dissolution Study

Figure 7 shows a comparison of the dissolution profiles of pure CEB powder, the physical mixture, CEB-loaded samples and the commercial product in PBS (pH 6.8, containing 1.0% SLS). The dissolution of formulations was evaluated at pH 6.8 because this more closely simulates fasting conditions in the small intestine, where absorption of the model drug is primarily expected to occur. The observed dissolution rate of pure CEB was considerably lower because of its poor aqueous solubility and large particle size. As seen from the dissolution profile, only about 43% of the pure CEB dissolved within 45 min compared with 82% for the commercial product. The simple mixture of CEB and MSU-FC showed no significant improvement in the dissolution rate of CEB compared with the pure CEB. However, the CEB-loaded MSU-FC formulation showed a significant improvement in the dissolution rate of CEB compared with the pure CEB or the commercial product. Remarkably, approximately 100% of the drug dissolved from CEB-loaded MSU-FC formulation within 20 min, as opposed to only 24% and 61% for the pure CEB and commercial product. This outstanding increase in drug dissolution may be largely attributed to the marked dispersing effect of the pores of MSU-FC transforming the crystalline state of CEB into an amorphous state (as confirmed by DSC and XRPD studies). Meanwhile, a high specific surface area of CEB-loaded MSU-FC was also beneficial for drug release. According to the Nernst–Brunner/Noyes–Whitney equation, the dissolution rate is proportional to the surface area available for dissolution (6,21,43). The specific surface area of drug-loaded MSU-FC (271.8 m^2/g) was approximately 298-fold higher than that of pure CEB powder (0.91 m^2/g). In addition, the particle sizes of the amorphous drug incorporated in the pore channels (nano-scale) were significantly reduced compared with that of pure crystalline CEB. It is obvious that drug particles in the nanometer size range will dissolve more rapidly than bulk drug (14,24,33). However, the CEB-loaded samples prepared by different carriers can also exhibit differences in their manner of dissolution. It was found that the dissolution rate of CEB from MSU-FC was faster than that from CMK-3. The CEB-loaded CMK-3 exhibits a typical sustained-release pattern in dissolution medium. As seen from the dissolution profile, only about 67% of the drug dissolved

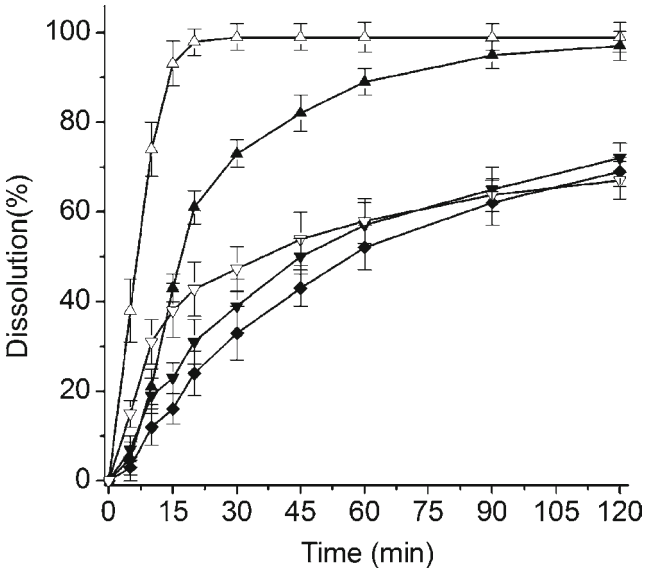

Fig. 7 Dissolution profiles of CEB from (◆) pure CEB, (▼) physical mixture, (▼) Celebrex® capsule, (△) CEB-MSU-FC and (▽) CEB-CMK-3 in PBS (pH 6.8, containing 1.0% SLS). Each data point represents the mean ± SD of three determinations.

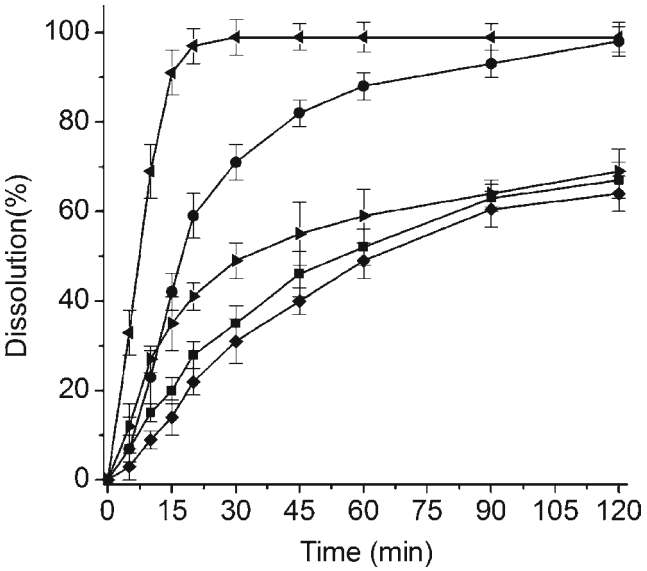

Fig. 8 Dissolution profiles of CEB from (◆) pure CEB, (■) physical mixture, (●) Celebrex® capsule, (◀) CEB-MSU-FC and (▶) CEB-CMK-3 in PBS (pH 1.2, containing 1.0% SLS). Each data point represents the mean ± SD of three determinations.

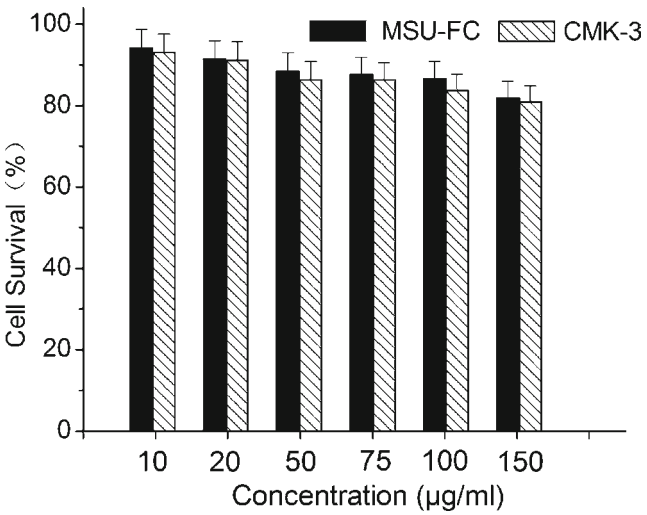

Fig. 9 Effect of MSU-FC and CMK-3 on the Caco-2 cell survival at various concentrations.

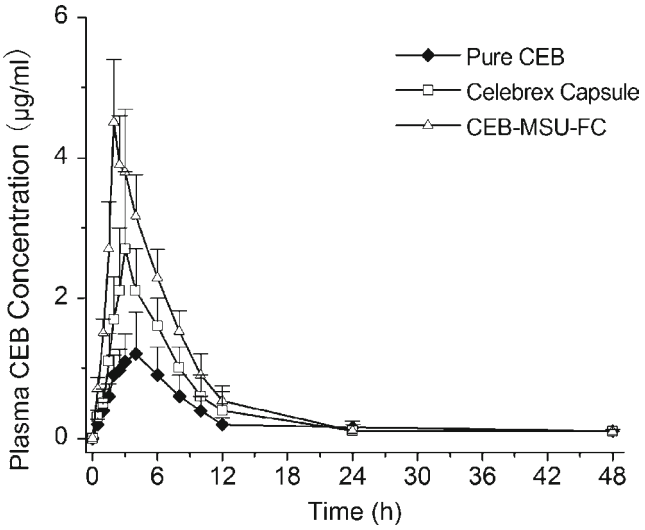

Fig. 10 Average plasma-drug concentration of CEB following single dose oral administration of different formulations to Sprague–Dawley rats ($n = 6$).

from CEB-loaded CMK-3 within 120 min compared with 100% for the CEB-loaded MSU-FC. The difference in the matrix architecture, including the pore diameter, the pore connectivity and geometry, may be responsible for the difference in the drug dissolution rate of the two different types of the CEB-loaded particles (25,30,44). MSU-FC possesses a highly accessible, three-dimensional pore network and a relatively larger pore diameter (26.0 nm) compared with CMK-3 (as confirmed by TEM and nitrogen adsorption studies). CEB molecules loaded into three-dimensional pore systems had a greater chance of escaping from pore channels and diffusing into the dissolution medium. In contrast, CMK-3 exhibited steric diffusion hindrance caused by the two-dimensional ordered channels and smaller pore entrance, thus preventing the easy diffusion of CEB molecules into the dissolution medium (21,28). In addition, the particle size of mesoporous carbon also has a great impact on the drug release characteristics. Monodispersed MSU-FC (~800 nm) with a smaller particle size possesses short pore channels and more pore entrances to release drug than agglomerated CMK-3 (1–4 μm) with a larger particle size (shown in Fig. 3). The relatively small particle size significantly reduced the pathway CEB needed to escape from the inner pores, thus contributing to the fast drug release profile (45). The effect of the CEB-loaded MSU-FC formulation on the CEB dissolution rate in hydrochloric acid solution (pH 1.2, containing 1.0% SLS) is shown in Fig. 8. The dissolution rate of CEB from the CEB-loaded MSU-FC formulation was significantly faster compared with that of pure CEB and other CEB formulation. As seen from the dissolution profile, only about 21% of the pure CEB dissolved within 20 min compared with approximately 100% for the CEB-loaded MSU-FC. Therefore, it is anticipated that MSU-FC is an excellent drug delivery vehicle for the fast release of poorly water-soluble drugs.

In Vitro Cytotoxicity Assay

Figure 9 shows the percentage survival of Caco-2 cells after continuous (24 h) exposure to different concentrations of carbon matrices. The cytotoxicity of both carbon matrices was found to be slightly concentration-dependent. However, both MSU-FC and CMK-3 matrices showed, at the concentrations tested (from 10 to 150 μg/ml), no significant cytotoxic effect on Caco-2 cells. Particularly, the percentage surviving cells did not fall below 90% even after incubating the cells with 100 μg/ml MSU-FC, indicating that the prepared MSU-FC nanomatrix is biocompatible. As evident from the cell survival data, there was no significant difference in cytotoxicity between MSU-FC and CMK-3 at the tested concentrations.

In Vivo Absorption Study

The observations on the rapid dissolution and increased saturation solubility properties of the CEB-loaded MSU-FC formulation prompted us to clarify the possible improvement in absorption of CEB, and so the pharmacokinetic behaviors of CEB-loaded MSU-FC, the commercial Celebrex® capsules and the pure CEB were assessed in Sprague–Dawley rats under the fasting condition. Plasma drug concentrations as a function of time were plotted and are shown in Fig. 10. The three plasma drug concentration profiles showed that CEB was completely eliminated from the plasma within 48 h, which indicated that the experimental time period selected was sufficient to assess the absorption characteristics of the different preparations. It is obvious from Fig. 10 that the drug absorption was highest from the CEB-loaded MSU-FC particles. The maximum plasma concentration (C_{max}) for this preparation was significantly higher ($p < 0.05$) than that of the other two preparations (4.52 ± 0.93 μg/ml *versus* 2.81 ± 1.02 μg/ml for

Table III Mean and Standard Deviation Values of the Pharmacokinetic Parameters of CEB Formulations After Oral Administration to Sprague–Dawley rats ($n = 6$)

Parameter	CEB-MSU-FC	Pure CEB	Celebrex Capsule
T_{max} (h)	1.75 ± 0.23 *	3.83 ± 0.41*	2.92 ± 0.58
C_{max} (μg/ml)	4.52 ± 0.93*	1.19 ± 0.67*	2.81 ± 1.02
$AUC_{0\rightarrow48h}$ (μg·h/ml)	26.38 ± 5.07*	7.86 ± 2.04*	15.42 ± 3.90
Relative bioavailability (%)	172.31 ± 36.8	50.46 ± 14.33	–

* $P < 0.05$ compared with the Celebrex capsule

Celebrex® and 1.19±0.67 μg/ml for pure CEB). Meanwhile, the time to reach the maximum plasma concentration (T_{max}) for this preparation was significantly shorter than for the other two preparations. The pharmacokinetic parameters of CEB obtained by the non-compartmental method are listed in Table III. The total area under the plasma concentration–time curve (AUC_{0-t}) which reflects the total amount of drug absorbed over the 48 h time period was also found to be significantly higher ($p<0.05$) for the CEB-loaded MSU-FC preparation than for the other two preparations (26.38±5.07 μg·h/ml compared with 15.42±3.90 μg·h/ml for Celebrex® and 7.86±2.04 μg·h/ml for pure CEB). Both the AUC_{0-t} and C_{max} values of the CEB-loaded MSU-FC preparation were markedly higher than those of the Celebrex® preparation, while the T_{max} was shorter, indicating a higher rate and extent of absorption. Compared with the commercial formulation, the relative bioavailability judged from the $AUC_{0\rightarrow 48h}$ of CEB was found to be 172.31±36.8% ($p<0.05$). The relative oral bioavailability of the CEB-loaded MSU-FC reflects the greatest *in vitro* drug dissolution from this formulation (Fig. 7). This indicates that the improvement in the relative oral bioavailability of CEB-loaded MSU-FC may be due to a higher drug dissolution rate in the GI tract following oral administration.

CONCLUSION

In the current study, a novel mesoporous carbon matrix, MSU-FC, with a large pore size (about 26 nm) and a three-dimensional porous structure was successfully prepared and used as a drug delivery vehicle. Characterization demonstrated the outstanding features of MSU-FC, including a high surface area, large pore volume, a well defined pore size distribution, making it an excellent drug carrier. CEB incorporation into the prepared MSU-FC resulted in an approximately 9-fold increase in aqueous solubility in comparison with crystalline CEB. The *in vitro* dissolution study showed that MSU-FC produced accelerated immediate release of CEB in comparison with crystalline CEB (pure CEB power or marketed formulation) and the drug-loaded CMK-3. The *in vivo* absorption study in fasted rats demonstrated that drug-loaded MSU-FC nanoparticles could improve the absorption of CEB, that is, 1.72-fold higher than the CEB commercial product. In addition, both MSU-FC and CMK-3 exhibited very low toxicity in the cytotoxicity assays, confirming the safety of mesoporous carbon when used as a drug delivery vehicle. Therefore, the MSU-FC nanomatrix has been shown to be a promising drug delivery vehicle for improving the dissolution and biopharmaceutical characteristics of poorly water-soluble drugs.

ACKNOWLEDGMENTS AND DISCLOSURES

This work was generously supported by the National Basic Research Program of China (973 Program) (No.2009CB930300). Dr. David B. Jack is gratefully thanked for correcting English of the manuscript.

REFERENCES

1. Hörter D, Dressman JB. Influence of physicochemical properties on dissolution of drugs in the gastrointestinal tract. Adv Drug Deliv Rev. 2001;46(1–3):75–87.
2. Lipinski CA, Lombardo F, Dominy BW, Feeney PJ. Experimental and computational approaches to estimate solubility and permeability in drug discovery and development setting. Adv Drug Deliv Rev. 1997;23(1–3):3–25.
3. Kawabata Y, Wada K, Nakatani M, Yamada S, Onoue S. Formulation design for poorly water-soluble drugs based on biopharmaceutics classification system: basic approaches and practical applications. Int J Pharm. 2001;420(1):1–10.
4. Lukyanov AN, Torchilin VP. Micelles from lipid derivatives of water-soluble polymers as delivery systems for poorly soluble drugs. Adv Drug Deliv Rev. 2004;56(9):1273–89.
5. Huanga LF, Tong WQT. Impact of solid state properties on developability assessment of drug candidates. Adv Drug Del Rev. 2004;56(3):321–34.
6. Kipp JE. The role of solid nanoparticle technology in the parenteral delivery of poorly water-soluble drugs. Int J Pharm. 2004;284(1–2):109–22.
7. Chen H, Khemtong C, Yang X, Chang X, Gao J. Nanonization strategies for poorly water-soluble drugs. Drug Discov Today. 2011;16(7–8):354–60.
8. Vasconcelos T, Sarmento B, Costa P. Solid dispersions as strategy to improve oral bioavailability of poor water soluble drugs. Drug Discov Today. 2007;12(23–24):1068–75.
9. LaVan DA, McGuire T, Langer R. Small-scale systems for in vivo drug delivery. Nat Biotechnol. 2003;21:1184–91.
10. Merisko-Liversidge E, Liversidge GG. Nanosizing for oral and parenteral drug delivery: a perspective on formulating poorly-water soluble compounds using wet media milling technology. Adv Drug Deliv Rev. 2011;63(6):427–40.
11. Eerdenbrugh BV, Mooter GV, Augustijns P. Top-down production of drug nanocrystals: nanosuspension stabilization, miniaturization and transformation into solid products. Int J Pharm. 2008;364(1):64–75.
12. Ghosh I, Bose S, Vippagunta R, Harmon F. Nanosuspension for improving the bioavailability of a poorly soluble drug and screening of stabilizing agents to inhibit crystal growth. Int J Pharm. 2011;409(1–2):260–8.
13. Constantinides PP, Chaubal MV, Shorr R. Advances in lipid nanodispersions for parenteral drug delivery and targeting. Adv Drug Del Rev. 2008;60(6):757–67.
14. Kesisoglou F, Panmai S, Wu Y. Nanosizing–Oral formulation development and biopharmaceutical evaluation. Adv Drug Del Rev. 2007;59(7):631–44.
15. Alexis F, Pridgen E, Molnar LK, Farokhzad OC. Factors affecting the clearance and biodistribution of polymeric nanoparticles. Mol Pharm. 2008;5(4):505–15.
16. Barbé C, Bartlett J, Kong L, Finnie K, Lin HQ, Larkin M, *et al*. Silica particles: a novel drug-delivery system. Adv Mater. 2004;16(21):1949–66.

17. Jaganathan H, Godin B. Biocompatibility assessment of Si-based nano- and micro-particles. Adv Drug Deliv Rev. 2012;64(15):1800–19.
18. Trewyn BG, Slowing II, Giri S, Chen HT, Lin VSY. Synthesis and functionalization of a mesoporous silica nanoparticle based on the sol–gel process and applications in controlled release. Acc Chem Res. 2007;40(9):846–53.
19. Yang F, Gai S, Lin J. Functionalized mesoporous silica materials for controlled drug delivery. Chem Soc Rev. 2012;41(9):3679–98.
20. Zhang Y, Wang J, Bai X, Jiang T, Zhang Q, Wang S. Mesoporous silica nanoparticles for increasing the oral bioavailability and permeation of poorly water soluble drugs. Mol Pharm. 2012;9(3):505–13.
21. Thomas MJK, Slipper I, Walunj A, Jain A, Favretto ME, Kallinteri P, *et al*. Inclusion of poorly soluble drugs in highly ordered mesoporous silica nanoparticles. Int J Pharm. 2009;387(1–2):272–7.
22. Zhang Y, Zhi Z, Jiang T, Zhang J, Wang Z, Wang S. Spherical mesoporous silica nanoparticles for loading and release of the poorly water-soluble drug telmisartan. J Control Release. 2010;145(3):257–63.
23. Li Z, Barnes JC, Bosoy A, Stoddart JF, Zink JI. Mesoporous silica nanoparticles in biomedical applications. Chem Soc Rev. 2012;41(7): 2590–605.
24. Wani A, Muthuswamy E, Savithra GHL, Mao G, Brock S, Oupický D. Surface functionalization of mesoporous silica nanoparticles controls loading and release behavior of mitoxantrone. Pharm Res. 2012;29(9):2407–18.
25. Vignolini S, Yufa NA, Cunha PS, Guldin S, Rushkin I, Stefik M, *et al*. A 3D optical metamaterial made by self-assembly. Adv Mater. 2012;24(10):23–7.
26. Ji X, Lee KT, Nazar LF. A highly ordered nanostructured carbon–sulphur cathode for lithium-sulphur batteries. Nat Mater. 2009;8: 500–6.
27. Liang C, Li Z, Dai S. Mesoporous carbon materials: synthesis and modification. Angew Chem. 2008;47(20):3696–717.
28. Wang X, Liu P, Tian Y. Ordered mesoporous carbons for ibuprofen drug loading and release behavior. Micropor Mesopor Mater. 2011;142(1):366–85.
29. Zhao P, Wang L, Sun C, Jiang T, Zhang J, Zhang Q, *et al*. Uniform mesoporous carbon as a carrier for poorly water soluble drug and its cytotoxicity study. Eur J Pharm Biopharm. 2012;80(3):535–43.
30. Heikkilä T, Salonen J, Tuura J, Hamdy MS, Mul G, Kumar N, *et al*. Mesoporous silica material TUD-1 as a drug delivery system. Int J Pharm. 2007;331(1):133–8.
31. Rosenholm JM, Lindén M. Towards establishing structure-activity relationships for mesoporous silica. J Control Release. 2008;128(2): 157–64.
32. Wang S. Ordered mesoporous materials for drug delivery. Micropor Mesopor Mater. 2009;117(1–2):1–9.
33. Vallet-Regí M, Balas F, Arcos D. Mesoporous materials for drug delivery. Angew Chem Int Edit. 2007;46(40):7548–58.
34. Tatsuda N, Yano K. Pore size control of monodispersed starburst carbon spheres. Carbon. 2013;51:27–35.
35. An S, Park JH, Shin CH, Joo J, Ramasamy E, Hwang J, *et al*. Well-dispersed Pd_3Pt_1 alloy nanoparticles in large pore size mesocellular carbon foam for improved methanol-tolerant oxygen reduction reaction. Carbon. 2011;49(4):1108–17.
36. Kwak G, Hwang J, Cheon JY, Woo MH, Jun KW, Lee J, *et al*. Preparation method of Co_3O_4 nanoparticles using ordered mesoporous carbons as a template and their application for fischer-tropsch synthesis. J Phys Chem C. 2013;117(4):1773–9.
37. Dolenc A, Kristl J, Baumgartner S, Planinšek O. Advantages of celecoxib nanosuspension formulation and transformation into tablets. Int J Pharm. 2009;376(1–2):204–12.
38. Paulson SK, Vaughn MB, Jessen SM, Lawal Y, Gresk CJ, Yan B, *et al*. Pharmacokinetics of celecoxib after oral administration in dogs and humans: effect of food and site of absorption. J Pharmacol Exp Ther. 2001;297(2):638–45.
39. Zhang Y, Zhang J, Jiang T, Wang S. Inclusion of the poorly water-soluble drug simvastatin in mesocellular foam nanoparticles: Drug loading and release properties. Int J Pharm. 2011;410(1–2):118–24.
40. Yan X, He P, Xia Y. Preparation of mesocellular carbon foam and its application for lithium/oxygen battery. Electrochem Commun. 2009;11(6):1127–30.
41. Yu L. Amorphous pharmaceutical solids: preparation, characterization and stabilization. Adv Drug Deliv Rev. 2001;48(1):27–42.
42. Skinner LM, Sambles JR. The Kelvin equation—a review. J Aerosol Sci. 1972;3(3):199–210.
43. Noyes AS, Whitney WR. The rate of solution of solid substances in their own solutions. J Am Chem Soc. 1897;19(12):930–4.
44. Horcajada P, Rámila A, Pérez-Pariente J, Vallet-Regi M. Influence of pore size of MCM-41 matrices on drug delivery rate. Micropor Mesopor Mater. 2004;68(1–3):105–9.
45. Cauda V, Muhlstein L, Onida B, Bein T. Tuning drug uptake and release rates through different morphologies and pore diameters of confined mesoporous silica. Micropor Mesopor Mater. 2009;118(1–3):435–43.